JOURNAL OF COMPUTATIONAL PHYSICS 3, 111–147 (1968)

A Global Numerical Ocean Model: Part I

W. P. CROWLEY

Lawrence Radiation Laboratory, University of California, Livermore, California 94550

Received March 27, 1968

ABSTRACT

This report describes a numerical model of the world oceans based on the primitive equations. The model ocean extends from 60° south to 60° north and is global in longitude. Continental boundaries are approximated by connecting mesh points with straight lines. For horizontal motions, the resolution allowed by the mesh is 5 deg. The vertical structure consists of six unevenly spaced layers which vary in size from 0.05 km at the surface to 0.8 km at the bottom. Bottom topography is ignored, but a free upper surface permits the existence of external gravity waves.

There are five prognostic variables (temperature, salinity, surface height anomaly, and two horizontal velocity components) which are functions of the four independent variables (latitude, longitude, depth, and time). Diagnostic variables are density anomaly, pressure, and vertical velocity. These are determined from the prognostic variables through an equation of state and the assumptions of hydrostatic equilibrium and incompressibility.

I. INTRODUCTION

In 1922, Richardson [1], [2] published a detailed description of his attempt to model large-scale atmospheric phenomena numerically. His was the first serious attempt to approach this problem from the numerical point of view, and he was unsuccessful primarily due to lack of computing power.

The development of electronics during World War II resulted in the birth of the high-speed electronic digital computer, which enabled Phillips [3] in 1956 to develop the first successful general circulation model. The rapid advance of computers and computer technology has led in the past five years to several "second generation" atmospheric models [4]–[9] some of which produce cine film records which reveal remarkably realistic weather-like motions over periods of days. Present day routine 24- and 48-hour predictions by the U.S. Weather Bureau are based on results from a simultation model aided at times by human interpretation.

All atmospheric models simplify the surface boundary condition to some extent. This simplification results in part from inadequate knowledge of the workings of the ocean-atmosphere boundary layer. To understand the energy transfer between the ocean and the atmosphere and thereby to develop more realistic atmospheric

models, it is necessary to model the ocean and eventually to couple the two models together. It is anticipated that by so doing, we will gain additional knowledge of the dynamics of the ocean itself.

Analytic theories of the wind-driven ocean circulation [10] have identified the causes of most of the apparent, large-scale oceanic phenomena such as the westward intensification of currents and the equatorial counter currents. Separate studies have also been made of thermohaline effects [11]–[13]. However, the real ocean is a time-dependent, three-dimensional nonlinear collage of these and other effects and in order to account for all the interactions one must eventually resort to numerical modeling. Pioneering work in this direction has been done by Bryan, [14], Sarkisyan [15], and others [16]–[19], who modeled the wind-driven circulation in different regions of the oceans. More recently Bryan and Cox [20] extended Bryan's model by including thermal effects.

This report (Part I) describes a global numerical ocean model presently under development. A later report (Part II) will contain results of calculations with the model.

The model is based on the primitive equations. At any time, each mesh-point in the ocean is characterized by a temperature, a salinity, and two horizontal velocity components. The surface height anomaly is also computed as a function of time and space. From these five prognostic variables, an equation of state, and the assumptions of incompressibility and hydrostatic equilibrium are derived the vertical velocity field and the internal pressure distribution.

The model ocean extends from 60° south to 60° north in latitude and is global in longitude. Continents are crudely approximated, but bottom topography is ignored, the ocean having a constant depth of 2 km which is divided into six unevenly spaced zones. The horizontal resolution is 5 degrees in latitude and in longitude.

Details of the model are presented in the following order. The mesh, coordinate system, and dependent variables are introduced in Section II. Sections III and IV give the basic equations and boundary conditions for the model. Since all external energy sources occur at the surface, the energy must be redistributed internally by physical processes. Two of these are dealt with in detail in Sections V (Vertical Convection) and VI (Eddy Diffusion). The finite difference approximations used are described in Section VII and a description of a calculation cycle is given in Section VIII. A list of symbols is given in Appendix A. The numerical technique used along lateral boundaries is discussed in Appendix B.

II. Coordinate System, Mesh, and Dependent Variables

The equations (see Section III) of the model are written relative to a spherical coordinate system rotating with angular velocity Ω. The longitudinal angle λ and its associated index k increase to the east from zero at Greenwich. The latitudinal

angle θ and its index l increase poleward from zero at the equator in each hemisphere. Meridians and parallels are thus k and l lines, respectively. The radial dimension z and its index m increase from a mean surface toward the center of the sphere. Thus the northern hemisphere forms a left-handed coordinate system, and the southern hemisphere forms a right-handed coordinate system.

Since this is a numerical model, the solutions of the equations of the model can be found in practice only at a finite number of points in the coordinate system. These points constitute the finite-difference mesh (or grid), and the physical separation of the points gives a lower bound to the scales of motion that can be explicitly computed with the model. On a surface z = constant (which will be loosely referred to as a horizontal surface) the mesh points are intersections of parallels with meridians and are separated by 5 deg in each direction. Due to the convergence of meridians in the poleward direction, the physical separation of k lines decreases from approximately 555 km at the equator to 278 km at 60 deg, where the mesh is terminated. The vertical structure consists of six layers with mesh points at z = 0.0, 0.05, 0.10, 0.20, 0.60, 1.20, and 2.0 km.

There are eight dependent and four independent variables in the model. Three of the dependent variables are derivable from the other five, and these three are known as the diagnostic variables. The remaining five variables are all time-dependent—their behavior is governed by partial differential equations. Since they are sufficient to determine the evolution of the model, they are known as the prognostic variables. The five prognostic variables are then temperature (T), salinity (S), east–west velocity ($u = a \cos\theta \, d\lambda/dt$), north–south velocity ($v = a \, d\theta/dt$), and surface height anomaly (z_s). Each of the first four is a function of the four independent variables; latitude, longitude, depth, and time. The surface height anomaly is a function only of latitude, longitude, and time, being defined only at the surface.

The diagnostic variables w (vertical velocity) and p (pressure) are evaluated from the prognostic variables at any particular time through equations arising from the assumptions of incompressibility and hydrostatic equilibrium. The third diagnostic variable σ (density anomaly) is an algebraic function of temperature, salinity, and depth.

For numerical purposes, the dependent variables are classified as being even, odd, or mixed. The odd prognostic variables, u and v, are centered between mesh points at $(k - \frac{1}{2}, l - \frac{1}{2}, m - \frac{1}{2}, n - \frac{1}{2})$ where n is the time index. Temperature and salinity are the even prognostic variables, and they as well as the diagnostic quantity σ are located at mesh points (k, l, m, n). The fifth prognostic variable, z_s, is even also, but is independent of depth and is thus located at the mesh points (k, l, n). The vertical velocity, being a vertical integral of a horizontal divergence of odd quantities occurs quite naturally at $(k, l, m, n - \frac{1}{2})$, while the pressure gradient is the horizontal derivative of a vertical integral of even quantities and is centered at $(k - \frac{1}{2}, l - \frac{1}{2}, m - \frac{1}{2}, n)$. These last two quantities are examples of mixed dependent variables.

III. EQUATIONS

At any time the state of the model is given by the eight variables u, v, T, S, z_s, w, p, and σ.

The temporal dependence of the model is governed by five partial differential equations for the tendencies of the prognostic variables u, v, T, S, and z_s. At any particular time, the other three variables are obtained from the prognostic variables through an equation of state and equations arising from the assumptions of incompressibility and hydrostatic equilibrium. Thus the model involves eight equations in eight unknowns.

The acceleration equations for a fluid particle in an inertial frame are, according to Newton's second law, obtained by equating the acceleration of the fluid particle to the net force per unit mass acting on the particle. Relative to a fixed spherical coordinate system, the equations are [24],

$$\frac{du}{dt} + \frac{\hat{u}\hat{w} - \hat{u}v \tan\theta}{r} = F_\gamma ,$$

$$\frac{dv}{dt} + \frac{\hat{w}v + \hat{u}^2 \tan\theta}{r} = F_\theta ,$$

$$\frac{d\hat{w}}{dt} - \frac{\hat{u}^2 + v^2}{r} = F_r .$$

Here θ is the latitudinal angle, γ is the longitudinal angle, $\hat{u} = r \cos\theta \, d\gamma/dt$, $v = r \, d\theta/dt$, and $\hat{w} = dr/dt$. The F's contain all the forces acting on the fluid particle and the substantial derivative is

$$\frac{dv}{dt} = \frac{\partial v}{\partial t} + \frac{\hat{u}}{a \cos\theta} \frac{\partial v}{\partial \gamma} + \frac{v}{a} \frac{\partial v}{\partial \theta} + \hat{w} \frac{\partial v}{\partial r} .$$

We transform to a coordinate system rotating with constant angular velocity Ω by defining a new longitudinal variable λ,

$$\lambda = \gamma - \Omega t.$$

With $u = r \cos\theta \, d\lambda/dt = \hat{u} - \Omega r \cos\theta$, the equations become

$$\frac{du}{dt} + \frac{u\hat{w} - uv \tan\theta}{r} - 2\Omega v \sin\theta + 2\Omega \hat{w} \cos\theta = F_\lambda ,$$

$$\frac{dv}{dt} + \frac{v\hat{w} + u^2 \tan\theta}{r} + (2u + r\Omega \cos\theta)\, \Omega \sin\theta = F_\theta ,$$

$$\frac{d\hat{w}}{dt} - \frac{u^2 + v^2}{r} - (2u + r\Omega \cos\theta)\, \Omega \cos\theta = F_r ,$$

where now the substantial derivative is

$$\frac{dv}{dt} = \frac{\partial v}{\partial t} + \frac{u}{a\cos\theta}\frac{\partial v}{\partial \lambda} + \frac{v}{a}\frac{\partial v}{\partial \theta} + \hat{w}\frac{\partial v}{\partial r}.$$

Expanding the forcing functions so as to expose the pressure terms and body forces,

$$F_r = -\frac{1}{\rho}\frac{\partial \hat{p}}{\partial r} - g + \bar{F}_r,$$

$$F_r + r\Omega^2\cos^2\theta = -\frac{1}{\rho}\frac{\partial \hat{p}}{\partial r} + \frac{1}{2}\frac{\partial}{\partial r}(r^2\Omega^2\cos^2\theta) - g + \bar{F}_r,$$

$$F_\theta = -\frac{1}{\rho r}\frac{\partial \hat{p}}{\partial \theta} + \bar{F}_\theta,$$

$$F_\theta - r\Omega^2\cos\theta\sin\theta = \frac{-1}{\rho r}\frac{\partial \hat{p}}{\partial \theta} + \frac{1}{2}\frac{1}{r}\frac{\partial}{\partial \theta}(r^2\Omega^2\cos^2\theta) + \bar{F}_\theta,$$

$$F_\lambda = -\frac{1}{\rho r\cos\theta}\frac{\partial \hat{p}}{\partial \lambda} + \frac{1}{2r\cos\theta}\frac{\partial}{\partial \lambda}(r^2\Omega^2\cos^2\theta) + \bar{F}_\lambda,$$

where the $\bar{F}$'s contain what remains of the forcing functions, namely the viscous terms. We now let $p = \hat{p} - \frac{1}{2}\rho r^2\Omega^2\cos^2\theta$ where the density variation is ignored and the equations become,

$$\frac{du}{dt} + \frac{u\hat{w} - uv\tan\theta}{r} - 2\Omega v\sin\theta + 2\Omega\hat{w}\cos\theta = -\frac{1}{\rho r\cos\theta}\frac{\partial p}{\partial \lambda} + \bar{F}_\lambda,$$

$$\frac{dv}{dt} + \frac{v\hat{w} + u^2\tan\theta}{r} + 2\Omega u\sin\theta = -\frac{1}{\rho r}\frac{\partial p}{\partial \theta} + \bar{F}_\theta,$$

$$\frac{dw}{dt} - \frac{u^2 + v^2}{r} - 2\Omega u\cos\theta = -\frac{1}{\rho}\frac{\partial p}{\partial r} - g + \bar{F}_r.$$

By including the centrifugal term due to the absolute rotation of the coordinate system in with the pressure term, we have essentially removed the constraint that the surface of the earth be a sphere. The $\cos^2\theta$ dependence indicates that the surface bulges at the equator relative to the poles.

Order of magnitude arguments reduce the third equation to the hydrostatic balance equation and allow the terms $v\hat{w}/r$ and $u\hat{w}/r$ to be dropped from the first two equations. In addition, we make the transformation to a vertical coordinate measured downward from the surface $r = a$,

$$z = a - r,$$

where a is the (assumed constant) radius of the earth's surface. Thus

$$w = dz/dt = -\hat{w}$$

and

$$\partial/\partial z = -\partial/\partial r$$

and the equations are

$$\frac{\partial u}{\partial t} = -\mathbf{V} \cdot \nabla u + fv + 2\Omega w \cos\theta - \frac{1}{\rho r \cos\theta}\frac{\partial p}{\partial \lambda} + Du, \tag{III-1}$$

$$\frac{\partial v}{\partial t} = -\mathbf{V} \cdot \nabla v - fu - \frac{1}{\rho r}\frac{\partial p}{\partial \theta} + Dv, \tag{III-2}$$

$$\partial p/\partial z = g\rho, \tag{III-2.1}$$

where $\mathbf{V}$ has components (u, v, w), $f = 2\Omega \sin\theta + (u/a)\tan\theta$ and Ω is the angular velocity of the "sphere" of radius a. The advective term for a vector component or a scalar, say ϕ, is given by

$$\mathbf{V} \cdot \nabla\phi = \frac{u}{a\cos\theta}\frac{\partial\phi}{\partial\lambda} + \frac{v}{a}\frac{\partial\phi}{\partial\theta} + w\frac{\partial\phi}{\partial z}.$$

The term Du represents an eddy diffusion of east–west momentum and is taken to be of the form

$$Du = \kappa\nabla_h^2 u + \frac{\partial}{\partial z}\kappa_v\frac{\partial u}{\partial z}.$$

It is recognized that this form for an eddy viscosity is inappropriate for flow on a sphere. For example, solid body rotation ($v = 0$, $u \propto \cos\theta$) results in a physically unacceptable diffusion of momentum. A more reasonable diffusion term would perhaps be based on the diffusion of angular momentum rather than linear momentum. The above eddy viscosity does however remove energy from scales comparable to the grid size, and thus it prevents the occurrence of nonlinear computational instabilities.

The vertical velocity field is obtained from an integral form of the incompressibility assumption

$$w(\lambda, \phi, \xi) = w(\lambda, \phi, H) + \int_H^{\xi} \mathscr{D}(\lambda, \theta, z')\, dz', \tag{III-3}$$

where $\mathscr{D}$ is the local horizontal divergence of the (u, v) field, here

$$\mathscr{D} = \frac{1}{a\cos\theta}\left[\frac{\partial u}{\partial\lambda} + \frac{\partial v\cos\theta}{\partial\theta}\right] = -\frac{\partial w}{\partial z}$$

and H is the depth of the ocean ($H = 2$ km). The upper limit of the integral is bounded by the inequality $z_s \leqslant \xi \leqslant H$.

If equation (III-3) is integrated over the surface of all oceans

$$\int_s w(\lambda, \theta, z_s)\, d\sigma = \int_s w(\lambda, \theta, H)\, d\sigma + \int_H^{z_s} \int_s \mathscr{D}(\lambda, \theta, z')\, d\sigma\, dz',$$

where $d\sigma = a^2 d\lambda d \sin\theta$, we find that there is no net change in the surface height. That is, ignoring evaporation and precipitation, volume is conserved.

The first integral on the right is zero since the integrand is taken to be identically zero as a boundary condition. The second integral is transformed by Green's theorem to,

$$\int_s \mathscr{D}(\lambda, \theta, z')\, d\sigma = \int_{P_1} ua d\theta + \int_{P_2} va \cos\theta\, d\lambda,$$

where P_1 consists of all boundary lines $\lambda =$ constant and P_2 consists of all boundary lines $\theta =$ constant. The boundary condition of zero normal velocity makes these last two integrals zero. Thus

$$\int_s w(\lambda, \theta, z_s)\, d\sigma = 0$$

and volume is conserved.

Since $w(\lambda, \theta, z_s)$ is not necessarily zero, an equation is needed to determine the evolution of the surface height as a function of latitude and longitude. The kinematic boundary condition $w(z_s) = dz_s/dt$ provides the necessary equation. Thus, the tendency of the surface height anomaly,[1] z_s, is

$$\partial z_s/\partial t = -\mathbf{V} \cdot \nabla z_s + w(z_s). \qquad \text{(III-4)}$$

A tendency equation for temperature is obtained by starting with the first law of thermodynamics in terms of specific enthalpy h. For a fluid particle, then,

$$dq = dh - \alpha dp,$$

where α is the specific volume. (Note that for adiabatic motions, the hydrostatic

[1] As indicated earlier, the earth is a rotating approximately oblate spheroid with the polar radius corresponding to the minor axis. The gravitational acceleration due to the earth's mass and the centrifugal acceleration due to the earth's rotation form a vector that is normal to the mean surface of this spheroid. This surface is given by $z = 0$; any differences between this system and a spherical coordinate system are ignored. The surface height anomaly z_s is then the local variation of the ocean's surface about $z = 0$ due to currents in the ocean.

assumption leads to conservation of the sum of enthalpy and potential energy in any column.) Assuming that $h = h(p, T)$,

$$dq = c_p\, dT + \left(\frac{\partial h}{\partial p} - \alpha\right) dp$$

and using the reciprocity relation $\partial h/\partial p)_T = \alpha - T\, \partial\alpha/\partial T)_p$,

$$dq = c_p\, dT - T\frac{\partial \alpha}{\partial T}\, dp = c_p\, dT - T\alpha\beta\, dp \qquad \text{(III-4.1)}$$

where

$$\beta = \frac{1}{\alpha}\frac{\partial \alpha}{\partial T}\Big)_p .$$

Using the hydrostatic equilibrium relation, $dp = \rho g\, dz$, replacing differentials with total time derivatives, noting that the vertical velocity is $w = dz/dt$, and introducing the mechanical equivalent of heat (J), we see that Eq. (III-4.1) becomes

$$\frac{dT}{dt} = \frac{1}{c_p}\frac{dq}{dt} + \frac{\beta g w}{J c_p} T,$$

where $\beta = \beta(T)$ as given in Fig. 1. Thus the tendency equation for temperature is, with $g/Jc_p = 2.35$ deg/km,

$$\frac{\partial T}{\partial t} = -\mathbf{V} \cdot \nabla T + \kappa_T \nabla_h{}^2 T + \frac{\partial}{\partial z}\kappa_{Tv}\frac{\partial T}{\partial z} + 2.35\beta w T \qquad \text{(III-5)}$$

and diabatic effects arise through horizontal and vertical eddy diffusion processes. That is,

$$\frac{1}{c_p}\frac{dq}{dt} = \kappa_T \nabla_h{}^2 T + \frac{\partial}{\partial z}\kappa_{Tv}\frac{\partial T}{\partial z} .$$

The tendency equation for salinity comes from mass conservation considerations. Considering only surface effects for the moment, we can write mass conservation as $d\rho/dt = -\partial G/\partial z$ where G[gm/cm^{2}sec] is a mass flux across the surface of the ocean, due to evaporation and precipitation. There is assumed to be no exchange of salt through the boundary layer connecting the atmosphere to the ocean, but the flux of water results in a salinity change. The salinity (gm/kg) is defined by $S = 1000\mathscr{S}$ where $\mathscr{S} = m_s/(m_s + m_w)$, and the average density in a zone of volume V is thus $\rho = m_s/\mathscr{S}V$. Since m_s is a constant, under the processes considered,

$$\frac{d(\rho \mathscr{S} V)}{dt} = \frac{dm_s}{dt} = 0.$$

Thus

$$\frac{d\mathscr{S}}{dt} = -\frac{\mathscr{S}}{\rho}\frac{d\rho}{dt} = \frac{\mathscr{S}}{\rho}\frac{\partial G}{\partial z} \text{ for } V = \text{constant},$$

or,

$$\frac{dS}{dt} = \frac{S}{\rho}\frac{\partial}{\partial z}G.$$

Upon introduction of advection and eddy diffusion, the salinity equation becomes

$$\frac{\partial S}{\partial t} = -\mathbf{V}\cdot\nabla S + \kappa_T\nabla_h^2 S + \frac{\partial}{\partial z}\kappa_{Tv}\frac{\partial S}{\partial z} \qquad \text{(III-6)}$$

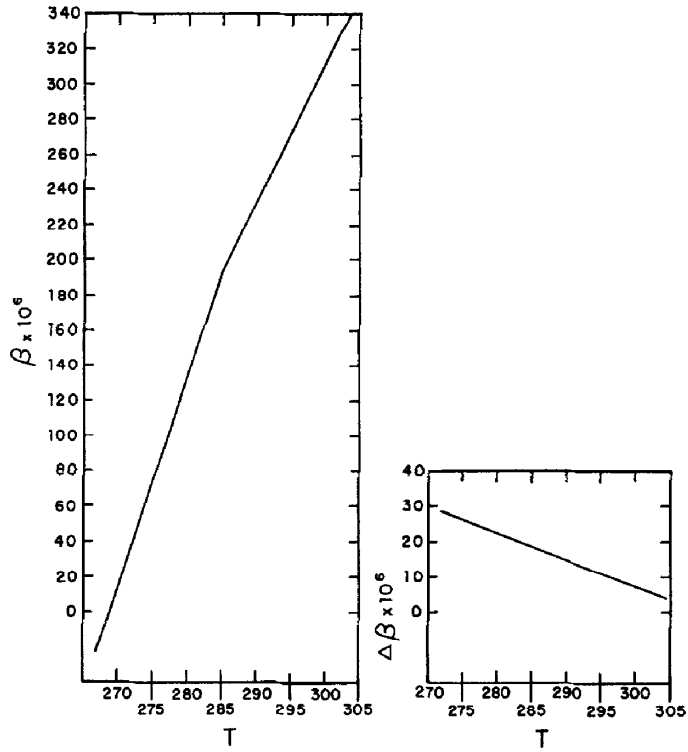

FIG. 1. The left curve is

$$\beta = \frac{1}{\alpha}\frac{\partial\alpha}{\partial T}\Big)_p$$

as a function of temperature at atmospheric pressure [22]. The right curve is a correction for depth, $\Delta\beta$ having units $°C^{-1}$ km^{-1}. The coefficient of thermal expansion at depth z is then $\beta + z\Delta\beta$.

where

$$\kappa_{Tv} \frac{\partial S}{\partial z}\Big)_{z=z_s} = \frac{S}{\rho} G.$$

The density anomaly at atmospheric pressure σ_T is an analytic function of temperature and salinity [21] given by

$$\sigma_T = 28.14 - 0.0735\,\overline{T} - 0.00469\,\overline{T}^2 + (0.802 - 0.002\,\overline{T})(S - 35),$$

where $\overline{T}$ is temperature in degrees Celsius, S is salinity in gm/kg and $\sigma = 10^3(\rho - 1)$. The density anomaly *in situ* is approximated by including a term which accounts for the slight compressibility of water,

$$\sigma = \sigma_T + 4.9107(z - z_s), \tag{III-7}$$

where z is the depth in km.

Hydrostatic equilibrium [Eq. (III-2.1)] allows the pressure gradient to be computed from

$$p(\xi) = p_s + g \int_{z_s}^{\xi} \rho(z')\, dz', \tag{III-8}$$

where $z_s \leqslant \xi \leqslant H$, and p_s is the surface pressure due to the weight of the atmosphere over the point in question. Thus, the east–west component of the pressure gradient at depth ξ is

$$\frac{\partial p(\xi)}{\partial \lambda} = \frac{\partial p_s}{\partial \lambda} + g \int_{z_s}^{\xi} \frac{\partial}{\partial \lambda} \rho(\lambda, \theta, z')\, dz' - g\rho_s \frac{\partial}{\partial \lambda} z_s(\lambda, \theta) \tag{III-9}$$

and a similar equation holds for the north–south component. It is seen then that the pressure term provides accelerations due to horizontal variations in surface pressure, in mass distribution, and in surface height. The contribution to the pressure gradient from variations in surface pressure and in surface height anomaly is independent of depth while the total gradient is a function of depth due to the internal variations in mass distribution.

The model is thus based on eight equations [Eqs. (III-1)–(III-8) excluding (III-4.1)] in eight unknowns. The equations are presented in the order in which they are solved. The methods of solution are dealt with in subsequent sections.

IV. Boundary Conditions

The boundary conditions fall naturally into two groups: (1) active or interactive boundary conditions at the surface, which include the driving mechanisms for the

ocean, and (2) passive lateral boundary conditions, which determine the physical boundaries of the flows generated.

The sea surface is a free boundary, subject to the kinematic boundary condition $w_S = dz_S/dt$, hence external gravity waves are not excluded from the model (they arise through the pressure gradient term $g\nabla z_s$ in the momentum equations). Since the minimal horizontal resolution is more than two orders of magnitude greater than the depth of the ocean, these gravity waves if they appear are shallow water waves and move with speed $(gH)^{1/2}$ or approximately 500 km/hr. There are also internal gravity waves present, but the speed of these waves is much less than that of the external gravity waves.

At the surface, the various mechanisms driving the ocean are introduced in terms of fluxes of momentum, water, and heat. Each of these quantities is determined at every surface mesh point as a function of local conditions.

The acceleration equations are affected by the gradient of atmospheric surface pressure [Eq. (III-9)] and surface stresses (which come from the empirical "square law" $\tau^x = -\rho C_D \mid V \mid u_a$ (see Ref. [22]).

$$\kappa_v \frac{\partial u}{\partial z}\Big)_{z=z_s} = \frac{1}{\rho}\tau^x = -C_D \mid V \mid u_a . \tag{IV-1}$$

$$\kappa_v \frac{\partial v}{\partial z}\Big)_{z=z_s} = \frac{1}{\rho}\tau^y = -C_D \mid V \mid v_a , \tag{IV-2}$$

where C_D is the drag coefficient, $\mid V \mid^2 = u_a^2 + v_a^2$, and u_a and v_a are the 1000-millibar winds. Balancing the surface stress against the momentum flux into the uppermost of the six vertical zones allows a surface current (u_s , v_s) to be estimated:

$$\frac{2\kappa_v(u_{1\frac{1}{2}} - u_s)}{z_2 - z_1} = -C_D \mid V \mid u_a . \tag{IV-3}$$

Here $u_{1-1/2}$ is the east-west velocity component at a depth of 12.5 meters, i.e., between the surface ($m = 1$) and the first interior mesh point ($m = 2$). A similar equation holds for v_s, which results in

$$\begin{aligned} u_s &= u_{1\frac{1}{2}} + (z_2 - z_1)\, C_D \mid V \mid u_a/2\kappa_v , \\ v_s &= v_{1\frac{1}{2}} + (z_2 - z_1)\, C_D \mid V \mid v_a/2\kappa_v . \end{aligned} \tag{IV-4}$$

Values of the drag coefficient and vertical eddy viscosity coefficient currently being used in the model are $C_D = 6 \times 10^{-6}$ and $\kappa_v = 3.6 \times 10^{-5}$ km^2/hr (100 cm^2/sec).

The surface source term in the salinity equation is the difference between the

precipitation ($\dot{P} \geqslant 0$) and evaporation rates, the precipitation is a given rate, and the evaporation rate is determined from

$$f_w = -C_w \mid V \mid (\mu_s - \mu_a), \tag{IV-5}$$

where μ_a is the water–vapor mixing ratio at 1000 millibars and μ_s is the saturation value of the water–vapor mixing ratio at the local surface temperature (μ_s is a tabulated function of temperature).

$$\kappa_{Tv} \frac{\partial S}{\partial z}\Big)_{z=z_s} = S(\dot{P} + f_w) \tag{IV-6}$$

The heat source at the surface includes net radiation ($\dot{I} - \dot{R}$ = insolation − net outward terrestrial radiation), heat lost through evaporation, and sensible heat transfer, which is

$$f_h = -C_h \mid V \mid (T - T_a), \tag{IV-7}$$

where T_a is the 1000-millibar air temperature. Thus the (negative) heat flux into the surface is

$$\kappa_{Tv} \frac{\partial T}{\partial z}\Big)_{z=z_s} = \dot{R} - \dot{I}(1 - A) + \frac{L}{c_p} f_w + f_h\,. \tag{IV-8}$$

The albedo A of the surface is taken to be zero (it is on the average approximately 7 % for Fresnel reflection from a smooth surface, but this is complicated by waves). All insolation reaching the ocean surface is assumed to be absorbed in the top 12.5 meters of the sea; this is in reasonable agreement with Pivovarov [23] who states that basically only the visible part of the spectrum penetrates beyond the top 50 cm and that even this is rapidly attenuated.

Lateral boundaries occur at 60 deg north and 60 deg south as well as along continental outlines. These boundaries are formed by connecting mesh points with straight lines so that the continents are at best crudely represented. The horizontal mesh and the lateral boundaries are shown in a world diagram (Fig. 2). Land (i.e., nonocean) regions appear stippled, and these regions are ignored in the calculation.

The lateral boundary conditions on temperature and salinity are of the insulating type. For momentum they are of the inviscid, slip type, so that the normal component of velocity is zero as is the shear. These boundary conditions are also imposed at noncontinental boundaries at 60 deg north and 60 deg south. Numerical techniques employed along lateral boundaries are discussed in Appendix B.

On the floor of the ocean, the normal temperature and salt fluxes are set zero (insulating boundary condition) as are the momentum flux and the vertical velocity [$w(H) = 0$].

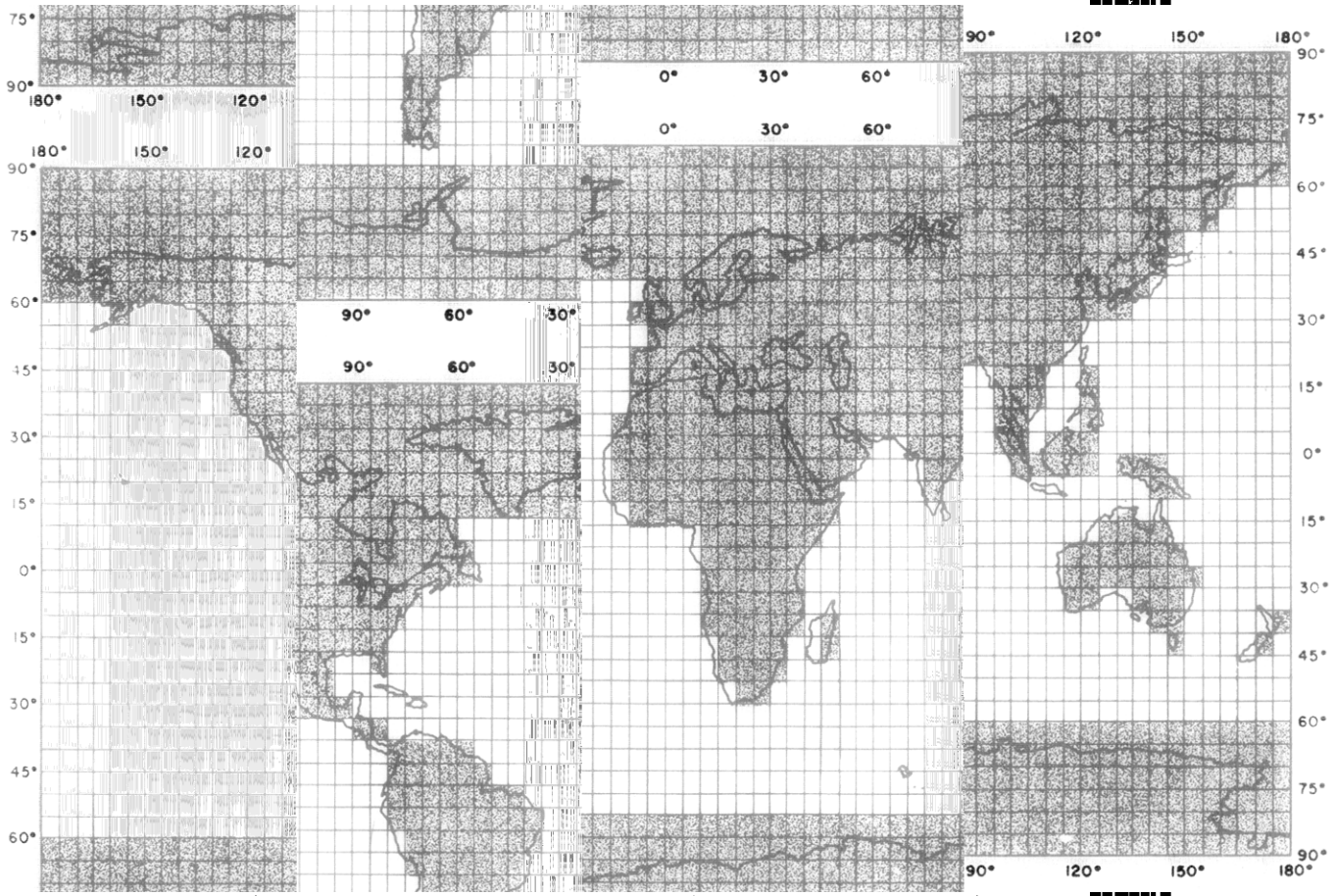

FIG. 2. A diagram of the continental boundary approximation used in the model. Horizontal and vertical lin[redacted]pond to I and k lines. Non-ocean regions are stippled—those regions are ignored in the calculations.

According to these boundary conditions, the model ocean is a fluid constrained to lie on a sphere between two parallels. It is subdivided into a number of connected basins by continents and is being driven by fluxes of heat, water, and momentum, all of which are introduced in the surface layer.

Energy deposited in surface layers is redistributed throughout the ocean by advective currents and by eddy diffusion processes. The horizontal eddy diffusion is usually proportional to the negative gradient of the quantity being diffused, the coefficient of proportionality being a constant. For momentum, a more complex prescription is used; this is discussed below in the section on eddy diffusion. Vertical diffusion is complicated somewhat by the presence of a gravitational field; this is discussed further in the next section.

V. Vertical Convection

For the most part, the vertical structure of the real ocean is stable. It does, however, attain an unstable configuration when the vertical density gradient becomes less than some (positive) critical gradient. This situation can occur at any level, but it is more likely to happen in the surface layers where it is instigated by the relative balance of heat fluxes with evaporation and precipitation. For example, in regions where there is an excess of evaporation over precipitation, the accompanying increase in surface water salinity causes a corresponding density increase. The unstable situation can also occur in regions where there is a net loss of heat from the surface water to the atmosphere. The cooling surface water will then tend to become heavier than the underlying, warmer water. This is a very noticeable effect in high-latitude waters during the winter months. Due to the extreme net heat loss (even during daylight hours) these winter waters are very unstable and lack both a thermocline and a halocline. In tropical waters, the cooling of surface water at night may lead to instabilities in this region also, but this is a diurnal effect.

In nature, these unstable situations are held in check by small-scale convection currents [24]. In this model, the unstable situations are rectified by the inclusion of a nonlinear vertical diffusion coefficient, which is assumed to be a function of $(1/\rho)(\partial\sigma/\partial z)\,\Delta z$, a measure of the static stability. (We will use Δ to denote an *in situ* difference and δ to denote a change following a parcel of water.)

The density of sea water is a function of temperature, salinity, and pressure. Due to the slight compressibility of water, there is an adiabatic temperature increase with depth,

$$\frac{\Delta T}{\Delta z} = \frac{\beta g T}{J c_p} \tag{V-1}$$

so that a parcel of water moved adiabatically from z_1 to z_2 will realize a temperature change of

$$\delta T = \Delta T = \frac{\beta g T}{J c_p}(z_2 - z_1).$$

Thus a parcel at depth z when raised adiabatically to the surface will have a temperature

$$\theta = T - \delta T \tag{V-2}$$

where δT is roughly $\beta g T z / J c_p$. This then defines the potential temperature.

Consider a water column of constant salinity and potential temperature. The *in situ* temperature gradient is given by $\Delta T/\Delta z = \beta g T/J c_p$, and the column is said to be stable or in convective equilibrium. That is, a water parcel displaced in the vertical will find itself surrounded by water of the same temperature. Its motion will be neither amplified nor retarded since its density is that of the water it displaces.

Indifferent equilibrium is a special case, rarely if ever encountered. More generally, the salinity and potential temperature are functions of depth. If in the general case a displaced parcel is subjected to a restoring force by buoyant effects, the situation is said to be stable. Otherwise it is unstable.

Consider a parcel of density $\rho(T_1, S_1, p_1)$ originally at depth z_1 which is displaced adiabatically downwards to depth z_2. It finds itself surrounded by and displacing water of density $\rho(T_2, S_2, p_2)$. The condition for stability is then

$$\rho(T_1 + \delta T, S_1, p_2) < \rho(T_2, S_2, p_2). \tag{V-3}$$

Expanding the left side of Eq. (V-3) in a Taylor series,

$$\rho(T_1 + \delta T, S_1, p_2) = \rho(T_1, S_1, p_1) + \frac{\partial \rho}{\partial T}\delta T + \frac{\partial \rho}{\partial p}(p_2 - p_1), \tag{V-4}$$

and substituting Eq. (V-4) into Eq. (V-3), we obtain

$$\frac{\rho(T_2, S_2, p_2) - \rho(T_1, S_1, p_1)}{\rho} > \frac{1}{\rho}\frac{\partial \rho}{\partial T}\delta T + \frac{1}{\rho}\frac{\partial \rho}{\partial p}(p_2 - p_1).$$

Replacing $-(1/\rho)(\partial\rho/\partial T)$ with the coefficient of thermal expansion and $(1/\rho)(\partial\rho/\partial p)$ with the coefficient of compressibility, the condition for stability becomes

$$\Delta\rho/\rho > -\beta\delta T + K\Delta p$$

Substituting for δT from Eq. (V-1), and using the hydrostatic relation, the condition for stability in terms of the density anomaly is

$$\frac{\Delta\sigma}{\rho} > \left(-\frac{\beta^2 g T}{J c_p} + K\rho g\right) 10^3 \Delta z \tag{V-5}$$

Parameters characteristic of the upper tropical layers are

$$T = 300 \text{ deg},$$
$$\beta = 310 \times 10^{-6}/\text{deg},$$
$$K = 4500 \times 10^{-8}/\text{bar}.$$

For these values, the stability condition becomes

$$\Delta\sigma/\rho > (-6.7 + 440)\, 10^{-2} \Delta z$$

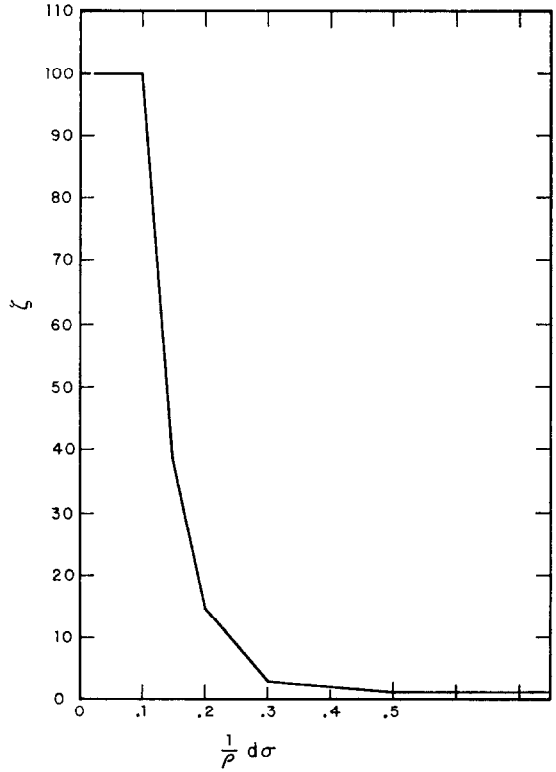

FIG. 3. The vertical diffusion coefficient $\kappa_{Tv} = \kappa_0 \zeta$ as a function of the vertical gradient of the density anomaly (κ_0 is a constant).

or

$$\Delta\sigma/\rho > 4.3\Delta z \tag{V-6}$$

where Δz is in km.

Thus unstable situations may occur even if lighter water lies above heavier water. In any case, if the *in situ* gradient of σ is less than some critical gradient, the stratification is unstable; in nature this gives rise to convection currents.

In the model, convection currents are statistically treated by specifying the vertical diffusion coefficient as a function of the vertical density gradient, $\kappa_{Tv} = \kappa_0\zeta$, where κ_0 is a constant and ζ, as a function of $\Delta\sigma/\rho$, is as given in Fig. 3. The functional dependence was established through numerical experiments with a one-dimensional (vertical) version of this model.

The arguments given here are based on the static stability of a column of water, and no allowance is made for the influence of current shear on stability [25], [26].

VI. Horizontal Eddy Diffusion

In this section both linear and nonlinear horizontal eddy viscosity coefficients are derived from notions about two-dimensional turbulence. (The ocean has a Reynolds number of 10^9, based on $U = 1$ km/hr, $H = 5$ km, and $\nu = 0.01$ cm^2/sec, and so is clearly in the turbulent domain of hydrodynamics.)

It has been known for some time that two-dimensional turbulent motions produce different spectra than three-dimensional turbulent motions [27]; the scale length separating these regimes is of the order of 10 km for the atmosphere and 5 km for the oceans. For small scale (i.e., three-dimensional) motions, the experimentally determined energy-density spectrum is proportional to $k^{-5/3}$ [28], [29]. This evidence is reinforced theoretically by the Kolmogorov hypotheses in which a constant energy-cascading rate $\epsilon[L^2T^{-3}]$ is assumed to exist in an inertial range (which separates the energy-containing range from the dissipation range) in wavenumber space. Dimensional arguments then give, for the energy density, $E[L^3T^{-2}]$,

$$E \propto \epsilon^{2/3}k^{-5/3}. \tag{VI-1}$$

An eddy viscosity $\kappa[L^2T^{-1}]$ which is a function of only ϵ and k is, dimensionally

$$\kappa \propto \epsilon^{1/3}k^{-4/3} \tag{VI-2}$$

so that, for $k^{-1} = 5$ km, and ϵ in the range 0.01 to 1.0 cm^2/sec (see Ref. [5]),

$$0.87 \times 10^7 < \kappa < 2 \times 10^7 \text{ cm}^2/\text{sec}.$$

With the horizontal mesh used in this model, the length-scale of explicitly computed horizontal motions has a lower bound of approximately 1000 km. Since the vertical length-scale is 5 km, the horizontal motions are clearly two-dimensional in nature; consequently one cannot resort to three-dimensional turbulence arguments for eddy viscosities. Fortunately, progress is now being made in the theory of two-dimensional turbulence, and eddy viscosities can be estimated on the basis of these theories.

In two-dimensional turbulence, there is, in addition to a constraint on energy, a constraint on vorticity [30]. By considering the conservation of mean squared vorticity as well as kinetic energy, Kraichnan [31] and Leith [32] arrived at the relation

$$E \propto \eta^{2/3} k^{-3}, \tag{VI-3}$$

where $\eta[T^{-3}]$ is the (assumed constant) cascading rate of mean squared vorticity. Using the three-dimensional case as a guide, we assume that the eddy viscosity is only a function of η and k, and deduce, dimensionally,

$$\kappa = \alpha \eta^{1/3} k^{-2}, \tag{VI-4}$$

where α is a constant. Unfortunately, η has not yet been determined experimentally, but it can be estimated from planetary vorticity considerations:

$$\begin{aligned} \eta &= \frac{\partial \omega^2}{\partial t} \cong \frac{v}{a} \frac{\partial \omega^2}{\partial \theta} \simeq \frac{v}{a} \frac{\partial}{\partial \theta} (2\Omega \sin \theta)^2 \\ &= (8\Omega^2 v/a) \sin \theta \cos \theta. \end{aligned} \tag{VI-5}$$

The choice of $v = 1$ km/hr and $\theta = \pi/4$ gives $\eta \cong 4.3 \times 10^{-5} \text{hr}^{-3}$. Then for $k^{-1} = 550/\pi = 175$ km, the eddy viscosity coefficient becomes

$$\kappa = 1070\alpha \text{ km}^2/\text{hr}.$$

An alternate approach is to estimate η locally (i.e., at each mesh point) as a function of the surrounding data, and to obtain in this manner a nonlinear viscosity. According to Leith [33], an estimate of η might be

$$\eta = \kappa(\nabla\omega) \cdot (\nabla\omega) \tag{VI-6}$$

where ω is the local vertical component of vorticity. Substituting Eq. (VI-6) into Eq. (VI-4),

$$\kappa = (\alpha^{1/2} L)^3 \mid \nabla\omega \mid, \tag{VI-7}$$

where L is a measure of the horizontal mesh size. Since we want no diffusion in the

limit of solid body rotation, ω should be the relative rather than the absolute vorticity.

In experiments with the model, both linear and nonlinear viscosities are being tested. For the linear case, the model will run without nonlinear computational instabilities developing if a viscosity coefficient of not less than 3600 km^2/hr (10^{10} cm^2/sec) is used. It is possible, however, to run with much smaller eddy diffusivities and values of $\kappa_T < 360$ km^2/hr are being tested. Thus eddy Prandtl numbers in excess of 10 are being used. Preliminary results from experiments with the nonlinear viscosity coefficient indicate that $\alpha \approx 2.4$ prevents the computational mode from developing.

VII. Finite Difference Equations

In this section, the numerical methods employed by the model are discussed. First, some general comments are made on the conversion of differential equations into finite difference equations. Then the numerical approximations to advection, diffusion, volume conservation, and the Coriolis acceleration are discussed and examined in the light of numerical stability considerations. Finally, the approximations to integrals for surface height anomaly and pressure are presented.

Ignoring for the moment the Coriolis term, the prognostic equations (Section III) are all of the form

$$\partial\psi/\partial t = -(A + B + ...)\,\psi, \tag{VII-1}$$

where $\psi = \psi(\lambda, \theta, z, t)$ is a scalar or a vector component and A, B,... are differential operators representing advection and diffusion. For example, if A represents east–west advection, $A\psi = (u/a\cos\theta)(\partial\psi/\partial\lambda)$. The transformation of Eq. (VII-1) into a difference equation is accomplished by first approximating the time derivative with a forward time difference[1],

$$\psi^{n+1} = \psi^n - \Delta t(A + B + ...)\,\psi^n. \tag{VII-1.1}$$

It would then seem to be a straightforward matter to replace the differential operators with stable difference approximations and to proceed to solve the resulting set of algebraic equations. It turns out, however, that even though the separate operator approximations may be stable, adding them together as in Eq. (VII-1.1) can cause computational instabilities to occur [6]. This difficulty is avoided by using an explicit version of Marchuk's method of time-splitting [34], so that Eq. (VII-1.1) is approximated by

$$\psi^{n+1} = (I - A_r)\cdots(I - A_2)(I - A_1)\,\psi^n, \tag{VII-1.2}$$

[1] For A, B,... independent of time, Eq. (VII-1) integrates to $\psi(t) = \epsilon^{t(A+B+\cdots)}\psi(0)$; Eq. (VII-1.1) thus has errors $0(\Delta t^2)$.

where now the A's are matrix representations of finite difference operators, and the factor of Δt has been absorbed.

Each of the separate operators in Eq. (VII-1.2) represents a different physical process (a different term in the differential equation) and the equation is solved in practice in a series of steps. For example, first $\psi^{n+1/r}$ is formed from

$$\psi^{n+1/r} = (I - A_1)\,\psi^n,$$

where $(I - A_1)$ may represent north–south advection. Then $\psi^{n+2/r}$ is formed,

$$\psi^{n+2/r} = (I - A_2)\,\psi^{n+1/r},$$

where $(I - A_2)$ may represent east–west advection. Finally,

$$\psi^{n+1} = (I - A_r)\,\psi^{n+1-1/r}.$$

(The fractional times between n and $n + 1$ have no physical interpretation.) Thus a sequence of one-dimensional operators has advanced ψ^n to ψ^{n+1}, and the numerical stability of Eq. (VII-1.2) is clearly assured if each operation is separately stable.

The model is however composed of a system of five differential equations, and the determination of a stability criterion for the system is more complicated than that stated above. In fact, the complete stability analysis would involve determining the eigenvalues of the fifth-order amplification matrix associated with the system of difference equations. Rather than proceed in that manner, we consider each physical process separately and arrive at a stability criterion for each separate case. From the separate criteria, a criterion for the system is estimated and this then permits a time step to be recommended. The procedure is justified *a posteriori* in that the model is numerically stable only when the recommended time step is not exceeded.

Consider advection on a mesh where the space increment (Δz) is not a constant. In Eq. (VII-1.2) this might be the result of the qth operator, giving the partially advanced function

$$\psi^{n+q/r} = (I - A_q)\,\psi^{n+(q-1)/r}. \tag{VII-2}$$

Physically, this step is modeled on the advection equation

$$\frac{\partial \psi}{\partial t} + w\frac{\partial \psi}{\partial z} = 0,$$

which expresses the idea that ψ is constant along characteristics of slope $1/w$ in the (z, t) plane.

If the $w^{n+1/2}$ field is known, a characteristic line (Fig. 4) may be passed through

the point $(m, n+1)$ intersecting the line $t = n\Delta t$ a distance $-w\Delta t$ from the point (m, n). Since ψ is assumed to be known at all m points at time $t = n\Delta t$, it can

accuracy dependent on the number of points used in the interpolation process. In particular, $\psi^*(\psi$ evaluated at $z^* = z_m - w\Delta t)$ can be estimated by passing the quadratic form $\psi = a + b(z - z_m) + c(z - z_m)^2$ through the three points ψ_{m-1}, ψ_m, ψ_{m+1} and evaluating the resulting expression at z^*. If $P = z_{m+1} - z_m$ and $Q = z_m - z_{m-1}$, the coefficients turn out to be

$$a = \psi_m,$$

$$b = \frac{Q^2\psi_{m+1} - P^2\psi_{m-1} - \psi_m(Q^2 - P^2)}{PQ(P+Q)},$$

$$c = \frac{Q\psi_{m+1} + P\psi_{m-1} - \psi_m(P+Q)}{PQ(P+Q)}.$$

and the advection process based on a quadratic fit is then given by

$$\psi_m^{n+1} = \psi^* = \psi_m^n + \frac{x(x+Q)}{P(P+Q)}(\psi_{m+1} - \psi_m) - \frac{x(x-P)}{Q(P+Q)}(\psi_m - \psi_{m-1})$$

where $x = -w^{n+1/2}\Delta t$. The operator for vertical advection is thus

$$(A\psi)_m = -\frac{x(x+Q)}{P(P+Q)}(\psi_{m+1} - \psi_m) + \frac{x(x-P)}{Q(P+Q)}(\psi_m - \psi_{m-1}). \tag{VII-3}$$

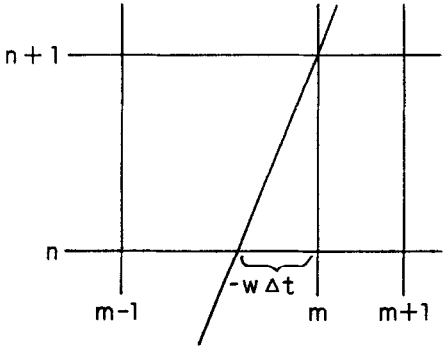

FIG. 4. Advection diagram.

Horizontal advection is carried out on a uniform mesh ($P = Q$), the operator becoming, in this case,

$$(A\psi)_j = \frac{\alpha}{2}(\psi_{j+1} - \psi_{j-1}) - \frac{\alpha^2}{2}(\psi_{j+1} - 2\psi_j + \psi_{j-1}), \qquad \text{(VII-4)}$$

where $\alpha = u\Delta t/a \cos\theta\Delta\lambda$ for east–west advection or $v\Delta t/a\Delta\theta$ for north–south advection.

The horizontal diffusion process may be approximated by

$$(A\psi)_j = -\beta(\psi_{j+1} - 2\psi_j + \psi_{j-1}), \qquad \text{(VII-5)}$$

where $\beta = \kappa\Delta t/\Delta x^2$. Since Eq. (VII-5) is similar in form to a part of Eq. (VII-4), for expediency horizontal advection and diffusion are combined under one operator,

$$(A\psi)_j = \frac{\alpha}{2}(\psi_{j+1} - \psi_{j-1}) - \left(\frac{\alpha^2}{2} + \beta\right)(\psi_{j+1} - 2\psi_j + \psi_{j-1}). \qquad \text{(VII-6)}$$

The stability analysis proceeds in a straightforward manner. An eigenvector $\epsilon^{ikj\Delta x}$ is substituted for ψ_j in Eq. (VII-6). This allows evaluation of the eigenvalues $\xi(k)$ of $(I - A)$. If $(I - A)$ is normal (i.e., it commutes with its Hermitian adjoint), a necessary and sufficient condition for stability is that ξ remain bounded by the unit circle [35]. Since $(I - A)$ is usually not normal, this condition is weakened to being only necessary, but in practice it seems to suffice. Performing the required operations, the eigenvalue of the operator $(I - A)$ in Eq. (VII-6) is found to be

$$\xi(k) = 1 - (\alpha^2 + 2\beta)(1 - \cos k\Delta x) - i\alpha \sin k\Delta x \qquad \text{(VII-7)}$$

and it follows that stability is assured by $\alpha^2 + 2\beta \leqslant 1$. Lax [36] has shown, for $\beta = 0$, that $|\alpha| \leqslant 1$ is a necessary and sufficient condition for stability of this advection prescription. The accuracy, amplitude damping, and phase error introduced by the advection part of this approximation are discussed elsewhere [37]. For the case of no advection ($\alpha = 0$), Eq. (VII-7) results in the usual stability criterion encountered in explicit diffusion calculations, namely $\beta \leqslant \frac{1}{2}$. For $\kappa = 3600$ km^2/hr, diffusion thus restricts the time step to 10.5 hr at a latitude of 60 deg.

Diffusion in the vertical direction is treated as a conserved flux, being modeled on the equation

$$\frac{d\psi}{dt} = -\frac{\partial F}{\partial z},$$

where

$$F = -\kappa_v(\partial\psi/\partial z).$$

The difference equations are thus (for fixed values of k and l),

$$F_{m-1/2} = -\kappa_{m-1/2} \frac{\psi_m - \psi_{m-1}}{z_m - z_{m-1}},$$

$$\psi_m^{n+1} = \psi_m^n - 2\Delta t \left(\frac{F_{m+1/2}^n - F_{m-1/2}^n}{z_{m+1} - z_{m-1}} \right), \tag{VII-8}$$

where $\kappa_{m-1/2}$ is obtained from Fig. 3. The stability requirement is $\kappa_v(\Delta t/\Delta z^2) < \frac{1}{2}$ which for $\kappa_0 = 1.8 \times 10^{-6}$ km^2/hr (5 cm^2/sec) leads to the restriction $\Delta t < 7$ hr. This constraint may be eliminated by writing implicit difference equations, but this additional complication is unnecessary at the present time.

In order to explicitly account for volume conservation (as discussed in Section III) in the numerical solution, Eq. (III-4) is rearranged before it is approximated by a finite difference expression. The quantity $z_s\mathscr{D}$ is added to and subtracted from the right-hand side to give

$$\frac{\partial z_s}{\partial t} = -\nabla_h \cdot \mathbf{V} z_s + z_s \mathscr{D} + w(z_s).$$

To obtain the difference approximation we first note that if the velocity components in $\mathscr{D}$ are chosen to be those centered at $m = 1\frac{1}{2}$ (ignoring the horizontal centering for the moment), the last two terms may be written

$$w_s + z_s\mathscr{D}_{1\frac{1}{2}} = w_2 + z_2\mathscr{D}_{1\frac{1}{2}} = w_7 + \sum_{m=7}^{3} \mathscr{D}_{m-1/2}(z_m - z_{m-1}) + z_2\mathscr{D}_{1\frac{1}{2}}, \tag{VII-8.1}$$

where Eq. (VII-15) has been used. To be consistent, the velocity components used for $\mathbf{V}$ must be those used for $\mathscr{D}$.

To evaluate the divergence term, we make use of Green's theorem,

$$\nabla_h \cdot \mathbf{V} z_s = \frac{1}{\Delta\sigma} \int (\mathbf{V} z_s) \cdot \mathbf{N} dl.$$

In finite difference form this expression becomes

$$\nabla_h \cdot \mathbf{V} z_s |_{k,l} \simeq \frac{1}{\Delta\sigma_{k,l}} [(F_{k+1/2,l} - F_{k-1/2,l})\, a\Delta\theta + (F_{k,l+1/2} \cos\theta_{l+1/2} - F_{k,l-1/2} \cos\theta_{l-1/2})\, a\Delta\lambda],$$

where

$$\Delta\sigma_{k,l} = a^2\Delta\lambda(\sin\theta_{l+1/2} - \sin\theta_{l-1/2})$$

$$2F_{k+1/2,l}\frac{\Delta t}{a\Delta\lambda\cos\theta_l} = \alpha_{k+1/2,l}[(z_s)_{k+1,l} + (z_s)_{k,l}] - \alpha^2_{k+1/2,l}[(z_s)_{k+1,l} - (z_s)_{k,l}]$$

$$2F_{k,l+1/2}\frac{\Delta t}{a\Delta\theta} = \gamma_{k,l+1/2}[(z_s)_{k,l+1} + (z_s)_{k,l}] - \gamma^2_{k,l+1/2}[(z_s)_{k,l+1} - (z_s)_{k,l}]$$

$$2\alpha_{k+1/2,l} = [u_{k+1/2,l+1/2,1\frac{1}{2}} + u_{k+1/2,l-1/2,1\frac{1}{2}}]\frac{\Delta t}{a\Delta\lambda\cos\theta_l}$$

$$2\gamma_{k,l+1/2} = [v_{k+1/2,l+1/2,1\frac{1}{2}} + v_{k-1/2,l+1/2,1\frac{1}{2}}]\frac{\Delta t}{a\Delta\theta}.$$

The fluxes defined above give second-order accuracy [37].

At each (k, l) point only two fluxes need be calculated, the other two being saved from similar preceeding calculations in adjacent zones. For boundary zones, the area, $\Delta\sigma$, must correspond to the fluid part of the zone and the fluxes across solid boundaries are merely set zero, corresponding to an application of the zero normal velocity boundary condition.

Upon splitting, the difference equation for z_s is

$$\begin{aligned}(z_s)^*_{k,l} &= (z_s)^n_{k,l} - \frac{a\Delta t\Delta\lambda}{\Delta\sigma_{k,l}}[F^n_{k,l+1/2}\cos\theta_{l+1/2} - F^n_{k,l-1/2}\cos\theta_{l-1/2}] \\ &\quad + \Delta t[w_2^{n+1/2} + z_2\mathscr{D}^{n+1/2}_{k,l,1\frac{1}{2}}] \\ (z_s)^{n+1}_{k,l} &= (z_s)^*_{k,l} - \frac{a\Delta t\Delta\theta}{\Delta\sigma_{k,l}}(F^*_{k+1/2,l} - F^*_{k-1/2,l}),\end{aligned} \tag{VII-9}$$

where F^n involves z_s^n and $v^{n+1/2}$ while F^* involves z_s^* and $u^{n+1/2}$.

Clearly the divergence part of the calculation can make no net contribution to the total volume of fluid since exactly that mass leaving one zone enters an adjacent zone and all normal boundary fluxes are set zero. It suffices then to show that

$$\sum_{k,l}(w_{k,l,2} + z_2\mathscr{D}_{k,l,1\frac{1}{2}})\,\Delta\sigma_{k,l} = 0$$

to demonstrate conservation of volume. From Eq. (VII-8.1) we have

$$\sum_{k,l}(w_{k,l,2} + z_2\mathscr{D}_{k,l,1\frac{1}{2}})\,\Delta\sigma_{k,l}$$

$$= \sum_{k,l} w_{k,l,7}\Delta\sigma_{k,l} + \sum_{m=7}^{3}(z_m - z_{m-1})\sum_{k,l}\mathscr{D}_{k,l,m-1/2}\Delta\sigma_{k,l} + z_2\sum_{k,l}\mathscr{D}_{k,l,1\frac{1}{2}}\Delta\sigma_{k,l}.$$

Since $w_7 \equiv 0$ and $\mathscr{D}$ is evaluated as the sum of fluxes (Eq. VII-14), the right-hand side of this expression is zero. We have, then

$$\sum_{k,l} (z_s)_{k,l}^{n+1} \Delta\sigma_{k,l} = \sum_{k,l} (z_s)_{k,l}^{n} \Delta\sigma_{k,l} .$$

The stability analysis of a linearized form of this equation provides only the restriction $\max(|\alpha|, |\gamma|) \leqslant 1$. A more meaningful analysis is carried out by considering a simplified version of this equation coupled to a simplified version of the acceleration equation. If we take as this system the linear equations

$$\frac{du}{dt} = -g\frac{\partial h}{\partial x}, \qquad \frac{dh}{dt} = -H\frac{\partial u}{\partial x},$$

and approximate them with the representative difference equations

$$u_{j-1/2}^{n+1/2} = u_{j-1/2}^{n-1/2} - g\frac{\Delta t}{\Delta x}(h_j^n - h_{j-1}^n),$$

$$h_j^{n+1} = h_j^n - H\frac{\Delta t}{\Delta x}(u_{j+1/2}^{n+1/2} - u_{j-1/2}^{n+1/2}),$$

the stability condition obtained is $(gH)^{1/2}(\Delta t/\Delta x) \leqslant 1$. Allowing for half zones at 60-deg. latitude, the restriction becomes $\Delta t < 0.25$ hr. For safety, the time step chosen for the model is 10 minutes. This allows the calculation to proceed (on the LARC computer) at 20 times real time.

The Coriolis acceleration couples the two momentum equations together. Consider

$$\frac{du}{dt} = fv, \qquad \frac{dv}{dt} = -fu,$$

where $f = 2\Omega \sin\theta$. Multiplying the first equation by u, the second by v and adding the two, results in

$$\frac{d}{dt}(u^2 + v^2) = 0, \tag{VII-10}$$

which is to say that, the Coriolis acceleration does not change the energy (since the force is normal to the displacement it does no work). This is used as a guide in choosing the numerical approximation for this process. Consider

$$\begin{aligned} u^{n+1} &= u^n + F[(1-\gamma)\, v^n + \gamma v^{n+1}], \\ v^{n+1} &= v^n - F[(1-\gamma)\, u^n + \gamma u^{n+1}], \end{aligned} \tag{VII-11}$$

where $F = f\Delta t$ and γ is an undetermined real parameter. Solving for the advanced velocities, and using matrix notation,

$$U = WV,$$

where

$$U = \begin{pmatrix} u^{n+1} \\ v^{n+1} \end{pmatrix}, \qquad V = \begin{pmatrix} u^n \\ v^n \end{pmatrix}$$

and

$$W = \begin{pmatrix} \dfrac{1 + F^2\gamma^2 - F^2\gamma}{1 + F^2\gamma^2} & \dfrac{F}{1 + F^2\gamma^2} \\ -\dfrac{F}{1 + F^2\gamma^2} & \dfrac{1 + F^2\gamma^2 - F^2\gamma}{1 + F^2\gamma^2} \end{pmatrix}.$$

Suppose that V is an eigenvector of W with corresponding eigenvalue λ. The energy at time $(n + 1)$ is given by the inner product

$$\langle U, U \rangle = \langle WV, WV \rangle = \lambda^2 \langle V, V \rangle$$

so that the energy guide amounts to the equality $\lambda^2 = 1$.

The magnitude of the eigenvalue of W is

$$|\lambda| = 1 + \frac{F^2 + F^4\gamma^2 - 2F^2\gamma(1 + F^2\gamma^2)}{(1 + F^2\gamma^2)^2}.$$

Satisfying the energy guide then leads to a cubic in γ having the three roots $1/2$, $+i/F$, $-i/F$. Since γ is a real parameter, the neutral case is thus given by $\gamma = 1/2$. Further analysis shows that $\gamma = 0$ (the explicit case) results in $|\lambda| > 1$ or growth, and $\gamma = 1$ (the fully implicit case) results in $|\lambda| < 1$, or damping.

Caution must be used in applying these results when the momentum equations contain accelerations in addition to the Coriolis terms. In the present case, the differential equations are Eq. (III-1) and Eq. (III-2) and the corresponding difference equations are

$$\begin{aligned} u^{n+1} &= u^* + F[(1 - \gamma)\, v^n + \gamma v^{n+1}], \\ v^{n+1} &= v^* - F[(1 - \gamma)\, u^n + \gamma u^{n+1}], \end{aligned} \qquad \text{(VII-12)}$$

where u^* and v^* are partially advanced values of u and v. That is, u^* and v^* contain the accelerations due to advection and diffusion for this time step.

Although in the preceeding analysis the neutral energy case came from a choice of $\gamma = 1/2$ in Eqs. (VII-11), this choice in Eq. (VII-12) can be shown to lead to computational energy growth for finite Δt. Similarly if in Eq. (VII-12), u^n and v^n are

replaced by u^* and v^*, the choice of $\gamma = 1/2$ also leads to computational energy growth.

The equations used in the model result from the choice of $\gamma = 1$, thus

$$u^{n+1} = (u^* + Fv^*)/(1 + F^2),$$
$$v^{n+1} = (-Fu^* + v^*)/(1 + F^2). \tag{VII-13}$$

While the numerical properties of this step can be determined only in very simple cases, the approximation used [Eqs. (VII-13)] seems to be stable in practice.

The horizontal pressure gradient is evaluated by numerically integrating Eq. (III-9) downward through the mesh starting with the surface condition,

$$\nabla_h p(0) = \nabla_h p_s - g\rho_s \nabla_h z_s$$

and using the approximation

$$I_{m-1/2} = \int_{m-3/2}^{m-1/2} \phi \, dz \simeq \frac{\phi_m}{8}(z_m - z_{m-1}) + \frac{3}{8}\phi_{m-1}(z_m - z_{m-2}) + \frac{\phi_{m-2}}{8}(z_{m-1} - z_{m-2})$$

which is obtained by assuming that ϕ varies linearly between "m" mesh points.

Thus

$$\nabla_h P)_{m-1/2} = \frac{1}{\rho_{m-1/2}}\left[\nabla_h p(0) + \sum_{i=2}^{m} I_{i-1/2}\right],$$

where

$$I_{2-1/2} = \frac{3\phi_1 + \phi_2}{8}(z_2 - z_s)$$

and

$$\phi = g\nabla_h \rho = 10^{-3} g \nabla_h \sigma.$$

In evaluating these terms, the ∇_h operator is replaced by the appropriate centered difference. Thus for example, the north–south gradient is

$$\nabla_h \sigma \,|_{k-1/2, l-1/2} = (\sigma_{k,l} + \sigma_{k-1,l} - \sigma_{k-1,l-1} - \sigma_{k,l-1})/2a\Delta\theta$$

which centers the term for the acceleration equations.

The vertical velocity field arises from a numerical integration of Eq. (III-3)

upward through the mesh starting with the boundary condition

$$w_7 = w(H) \equiv 0.$$

The divergence of the horizontal velocity field $\mathscr{D}$ is evaluated as a line integral (by Green's theorem), and is given by

$$\mathscr{D}_{k,l,m+1/2} = \frac{(v_1 + v_2)\cos\theta_{l+1/2} - (v_3 + v_4)\cos\theta_{l-1/2} + (u_1 + u_4 - u_2 - u_3)\,\Delta\theta/\Delta\lambda}{2a(\sin\theta_{l+1/2} - \sin\theta_{l-1/2})}. \tag{VII-14}$$

The notation comes from Fig. 5, so that $u_1 = u_{k+1/2,l+1/2,m+1/2}$, etc.

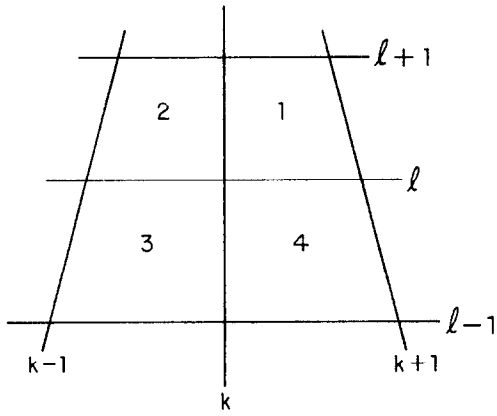

FIG. 5. Notation diagram for the horizontal divergence calculation.

Thus

$$w^{n+1/2}_{m,k,l} = \sum_{i=6}^{m} \mathscr{D}_{k,l,i+1/2}(z_{i+1} - z_i) \qquad \text{(summed backwards)}, \tag{VII-15}$$

where $\mathscr{D}_{k,l,i+1/2}$ is assumed constant in the interval from z_{i+1} to z_i.

VIII. Calculational Procedure

The current version of this model is running on the LARC, a decimal digital computer with 26,000 words of available high-speed memory and 26 fast registers. A word consists of 12 digits; if floating point arithmetic is used, there is a sign digit, an excess 50 exponent and a fraction of 9 digits. Memory may be extended by use of either magnetic tapes or drums, both of which can exchange information with

memory in a fully buffered manner. Drums are subdivided into 100 bands of 2500 words each; thus every drum has a capacity of 250,000 words.

At the beginning of a calculation cycle the prognostic variables are all stored on one drum with each l line (circle of latitude) residing on one band. This requires 25 bands. At the end of the cycle the values are on a different drum, having passed through memory and having been advanced from time step $n(n - 1/2)$ to $n + 1(n + 1/2)$. The three-point interpolation scheme currently used in the model requires that three l lines be in memory simultaneously. In addition two more lines are used to bring information from and to send information to the drums. That is to say, while calculating new information for line l, using lines $l + 1$, and $l - 1$, the next line $(l + 2)$ is being read in, and line $l - 2$ is being written out onto a different drum. The buffering capability is used, and since the compute time per l line turns out to be greater than the read/write time per l line the machine is computing all the time, having essentially free input/output.

Supposed then that lines $l - 1$, l, and $l + 1$ are in memory, and the summary orders have been issued to commence writing from $l - 2$ and reading into $l + 2$. If E and O stand for even (T, S, z_s) and odd (u, v) variables, we have in memory $E^{n-1}_{k,l,m}$ and $O^{n-1/2}_{k-1/2,l-1/2,m-1/2}$ for all m and k and for $l - 2$, $l - 1$, l, and $l + 1$. First, $w^{n-1/2}_{k,l,m}$ is formed by integrating the divergence of the horizontal velocity field. This then allows $z^n_{sk,l}$ to be formed for all k. Next, $E^n_{k,l,m}$ is computed based on the velocities and surface quantities at time $n - 1/2$. Then north-south advection and diffusion (for all m and k) are done for $O^{n-1/2}_{k-1/2,l-1/2,m-1/2}$, then vertical advection and diffusion (for all m and k), followed by east-west advection and diffusion (for all m and k). Finally, the acceleration terms are included (based on $E^n_{k,l,m}$ and $E^n_{k,l-1,m}$), and the result is $O^{n+1/2}_{k-1/2,l-1/2,m-1/2}$. This completes the calculation cycle, and, by this time, the new line $(l + 2)$ is in memory and the calculation can be repeated for $l + 1$.

The calculation starts at the equator and proceeds north to 60 deg. It then starts at the equator again and proceeds south to 60 deg. At this time, the original state (time t) has been advanced to time $t + \Delta t$ and the variables have been moved to another drum. The succeeding cycle advances the state of the model to $t + 2\Delta t$ and moves the information back to the original drum.

Periodically all variables are read from the current drum and written onto a magnetic tape for restart and editing purposes. A full tape can hold approximately 15 restart dumps.

APPENDIX A. Definitions of Symbols

A albedo of the sea surface
a radius of the earth (6366 km)
C_D drag coefficient

c_p specific heat (1 cal/gm deg)
$\mathscr{D}$ horizontal divergence of (u, v) field
f Coriolis parameter $(2\Omega \sin \theta + (u/a) \tan \theta)$
g acceleration due to gravity
H depth of model ocean (2 km)
h specific enthalpy
J mechanical equivalent of heat (4.1862×10^7 ergs/cal)
K coefficient of compressibility
k latitudinal index, also used as a wavenumber
l longitudinal index
L latent heat of evaporation (596 cal/gm)
m depth index
m_s mass of salt
m_w mass of water
n time index
p pressure
p_s surface pressure (due to atmosphere)
$\mathscr{S}$ $m_s/(m_s + m_w)$(gm/gm)
S salinity (gm/kg), $S = 1000\mathscr{S}$
T temperature (°K)
$\overline{T}$ temperature (°C)
t time (hr)
u east-west current (positive to east)
u_s surface current (u)
$\mathbf{V}$ vector current with components (u, v, w)
v north-south current (positive poleward)
v_s surface current (v)
w vertical current (positive downward)
z depth coordinate (positive downward)
z_s surface height anomaly
α specific volume
β coefficient of thermal expansion
ζ the part of the vertical diffusion coefficient dependent on stability
θ latitudinal angle, also used as potential temperature
κ horizontal eddy viscosity coefficient
κ_v vertical eddy viscosity coefficient
κ_T horizontal eddy diffusion coefficient
κ_{Tv} vertical eddy diffusion coefficient $(\kappa_{Tv} = \kappa_0\zeta)$
κ_0 vertical eddy diffusion coefficient for a stable configuration
λ longitudinal angle
μ water vapor mixing ratio

ρ density
σ density anomaly *in situ* [$\sigma = (\rho - 1)\, 10^3$]
σ_T density anomaly at atmospheric pressure
Ω angular velocity of the earth ($2\pi/24$/hr)
∇ gradient operator
∇_h horizontal gradient operator;

$$\nabla_h \cdot \mathbf{V} = \mathscr{D} = \frac{1}{a \cos\theta}\left[\frac{\partial u}{\partial \lambda} + \frac{\partial v \cos\theta}{\partial \theta}\right]$$

∇_h^2 horizontal Laplacian operator (approximate),

$$\nabla_h^2 \rho = \frac{1}{a^2 \cos^2\theta}\frac{\partial^2 \rho}{\partial \lambda^2} + \frac{1}{a^2}\frac{\partial^2 \rho}{\partial \theta^2}.$$

$\Delta\sigma$ horizontal area, $\Delta\sigma_{k,l} = a^2 \Delta\lambda\, (\sin\theta_{l+1/2} - \sin\theta_{l-1/2})$.

APPENDIX B. Numerical Techniques Used Along Lateral Boundaries

In this section the numerical technique used along lateral boundaries is discussed. technique is exemplified for situations involving advection and diffusion. Finally, the equation for the vertical velocity along lateral boundaries is obtained.

Two important assumptions are made concerning the lateral boundaries. The first is that continents have essentially precipitous coastlines. That is, along the coast line, the ocean is two km deep (subject to modification by the local value of z_s). There is no continental shelf in the model. The second assumption is that the "horizontal" aspects of the physical coast line can be approximated by a sequence of line segments connecting even (see below) mesh points. Each line segment is thus a 5-deg arc of a meridian or a parallel, and the ordered collection of line segments delimiting a land mass is called a boundary line. In Fig. 2 of the text, boundary lines separate clear (oceanic) regions from stippled (land) regions. Boundary lines also serve to terminate the mesh at 60° north and south.

Mesh points are classified even or odd, as are the dependent variables. Even mesh points occur at the intersection of k, l, and m lines, while odd mesh points are located at the points ($k - 1/2, l - 1/2, m - 1/2$). Since we are concerned only with the lateral boundaries, we will consider points on a surface z = constant with the understanding that the rules developed hold at each of these surfaces.

Each mesh point whether odd or even is further thought of as being either an exterior or an interior point. Exterior points coincide with continental or land regions and are ignored in the calculation. (They could, however, be used in an energy balance calculation to compute ground surface temperatures and moisture

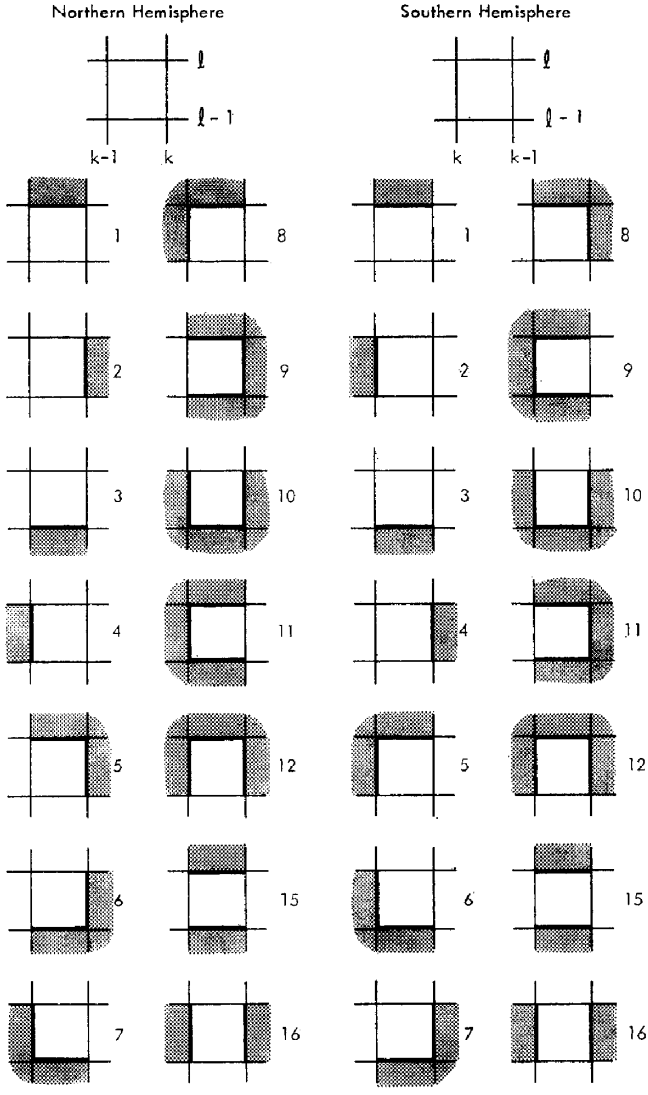

Fig. B-1. Indices for odd mesh points, Northern and Southern Hemispheres.

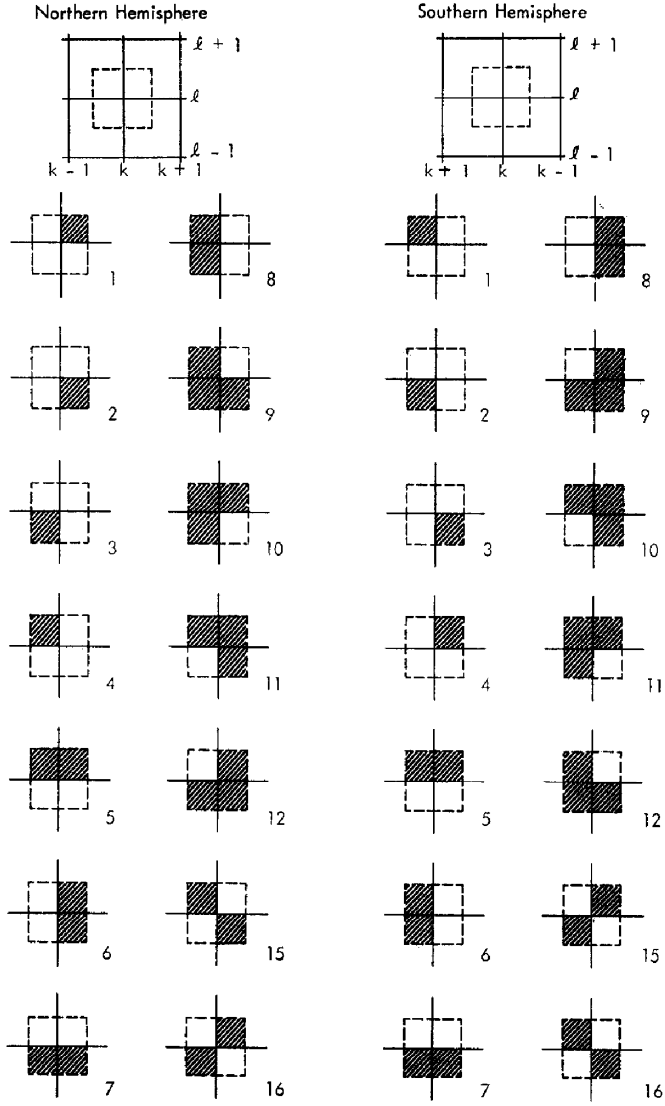

Fig. B-2. Indices for even mesh points, Northern and Southern Hemispheres.

content.) Interior points are those points at which the prognostic variables in the model are calculated each time step in accordance with the difference approximations to Eqs. (III-1), (III-2), (III-4), (III-5), and (III-6). Interior points, if within $2\frac{1}{2}$ deg of boundary lines, are called boundary points and require special attention with respect to the difference equations.

Since fluxes of the prognostic variables are specified along boundaries, the tendencies of quantities at boundary points are not necessarily zero. To compute these tendencies, the given boundary conditions are indirectly combined with the differential equations, and the tendencies are computed from this hybrid set of equations. This is accomplished by storing the appropriate data in unused exterior points that border boundary points. In this way the boundary conditions are satisfied and each boundary point is made to look like an interior point. For the most part then, only one difference equation has to be programmed for each differential equation.

Each mesh point is assigned an index based on the location and orientation of the nearest boundary line (Figs. B-1 and B-2). At each mesh point, then, the value of the index will determine the proper action to be taken so as to make that point appear to be an interior point. Exterior points have an index of 14; no calculation is done at these points. Interior points have an index of 13; no special preliminary setup is needed to calculate tendencies at these points.

As an illustrative example consider the northern hemisphere horizontal advection calculation for velocity at a point with an odd index of 5. According to Fig. B-1 (left portion) this point has a boundary line segment $2\frac{1}{2}$ deg to the east and another $2\frac{1}{2}$ deg to the north. An example of this type of point occurs in Fig. 2 of the text at $122\frac{1}{2}$ deg east longitude and $32\frac{1}{2}$ deg north longitude. According to the horizontal advection difference approximation (see Section VII), to evaluate

$$u \frac{\partial u}{\partial \lambda}\Big)_{k-1/2,l-1/2}$$

we need values of u at $(k - 3/2, l - 1/2)$, $(k - 1/2, l - 1/2)$ and $(k + 1/2, l - 1/2)$. The first two points are interior points at which u is known. The last point is determined from the boundary condition of no normal transport across lateral boundaries and this is satisfies by setting $u_{k+1/2,l-1/2}$ equal to $-u_{k-1/2,l-1/2}$. Similarly, to evaluate $v(\partial u/\partial\theta)$ at this same point we have u at points $(k - 1/2, l - 3/2)$ and $(k - 1/2, l - 1/2)$ and use the "no lateral shear" boundary condition to determine the third point; $u_{k-1/2,l+1/2}$ is set equal to $u_{k-1/2,l-1/2}$. Once these exterior points are set up, the terms $u(\partial u/\partial\lambda)$, $v(\partial u/\partial\theta)$, etc. are calculated by the equations in Section VIII. Fortunately, the same procedures hold for diffusion as well as advection.

As a second example, consider horizontal advection and diffusion of salinity in the southern hemisphere at a point with an even index of 5 [see Fig. B-2 (right

portion)]. The boundary condition of zero normal velocity at lateral boundaries means the term $v(\partial S/\partial\theta)$ is zero. The no-shear boundary condition allows the east–west velocity component to be approximated by

$$u_{k,l} = (u_{k-1/2,l-1/2} + u_{k+1/2,l-1/2})/2.$$

To approximate the north–south diffusion term, $(\kappa/a^2)(\partial^2 S/\partial\theta^2)$, we have S at the points $(k, l-1)$ and (k, l) and need it at $(k, l+1)$. The boundary condition on S (and T for that matter) is zero normal flux at all lateral boundaries. If it is assumed that the salinity flux is proportional to the negative gradient of S, the boundary condition is satisfied by setting $S_{k,l+1}$ equal to $S_{k,l-1}$.

The vertical velocity field is obtained at boundary points as well as at interior points from the divergence of the horizontal velocity field. Referring to Fig. 5 of the text for notation and recalling Green's theorem, we see that for an interior point

$$\mathscr{D}_{k,l} = [(u_1 + u_4 - u_2 - u_3)\Delta y + (v_1 + v_2)\Delta x_{l+1/2} - (v_3 + v_4)\Delta x_{l-1/2}]/2\Delta y\Delta x_l$$

where $\Delta y = a\Delta\theta$ and $\Delta x_l = a\cos\theta_l\Delta\lambda$. [This is a restatement of Eq. (VII-14).] The horizontal divergence at boundary points is computed correctly if velocities corresponding to exterior points are simply set zero in this equation, and if the area, $\Delta x\Delta y_l$ is taken to be that area corresponding to the fluid part of the zone.

For example, at a point in the northern hemisphere which has an index of 1, the horizontal divergence consistent with the velocity boundary conditions (zero shear, zero normal velocity) is, from Green's theorem,

$$\mathscr{D}_{k,l} = \left[u_4\frac{\Delta y}{2} + v_2\frac{\Delta x_{l+1/2}}{2} - (u_2 + u_3)\frac{\Delta y}{2} - (v_3 + v_4)\frac{\Delta x_{l-1/2}}{2}\right]\Big/\Delta y\Delta x_l$$

where $\Delta y\Delta x_l = (a^2\Delta\lambda/2)(\sin\theta_{l+1/2} + \sin\theta_l - 2\sin\theta_{l-1/2})$. This is obtained from Eq. (VII-14) if $u_1 = v_1 = 0$.

The vertical velocity field is then obtained by substituting $\mathscr{D}_{k,l,m-1/2}$ into into Eq. (VII-15).

ACKNOWLEDGMENTS

I am deeply indebted to Dr. C. E. Leith for advice and guidance rendered during all phases of the development of this model. I appreciate also the constructive criticism of the manuscript offered by Mrs. Barbara K. Crowley and Dr. Thomas F. Budinger. This work was done under the auspices of the U.S. Atomic Energy Commission.

REFERENCES

1. L. F. RICHARDSON, "Weather Prediction by Numerical Process." Cambridge University Press, London (1922); reissued by Dover, New York (1965).

2. G. PLATZMAN, A retrospective view of Richardson's book on weather prediction, *Bull. Am. Meteorol. Soc.* **48**, 514–550 (1967).

3. N. PHILLIPS, The general circulation of the atmosphere: A numerical experiment, *Quart. J. Meteorol. Soc.* **82**, 123–164 (1965).
4. A. KASAHARA AND W. WASHINGTON, NCAR global general circulation model of the atmosphere, *Monthly Weather Rev.* **95**, 389–402 (1967).
5. Y. KURIHARA AND J. HOLLOWAY, JR., Numerical integration of a nine-level global primitive equation model formulated by the box method, *Monthly Weather Rev.* **95**, 509–530 (1967).
6. C. LEITH, Numerical simulation of the Earth's atmosphere, *in* "Methods in Computational Physics," Vol. 4, pp. 1–18. Academic Press, New York (1965).
7. S. MANABE AND J. SMAGORINSKY, Simulated climatology of a general circulation model with a hydrologic cycle, *Monthly Weather Rev.* **95**, 155–169 (1967).
8. Y. MINTZ, Very long term integration of the primitive equations of atmospheric motion, *in* "World Meteorological Organization—International Union for Geodesy and Geophysics Symposium on Research and Developmental Aspects of Long-Range Forecasting, Boulder, Colorado, 1964," Technical Note No. 66 (1965), pp. 141–167.
9. J. SMAGORINSKY, General circulation experiments with the primitive equations. I. The basic experiment, *Monthly Weather Rev.* **91**, 99–164 (1963).
10. A. R. ROBINSON (Ed.), "Wind Driven Ocean Circulation." Blaisdell, New York (1962).
11. G. NEEDLER, A model for thermohaline circulation in an ocean of finite depth, *J. Marine Res.* **25**, 329–342 (1967).
12. A. ROBINSON AND H. STOMMEL, The oceanic thermocline and the associated thermohaline circulation, *Tellus* **11**, 295–308 (1959).
13. P. WELANDER, An advective model of the ocean thermocline, *Tellus* **11**, 309–318 (1959).
14. K. BRYAN, A numerical investigation of a nonlinear model of a wind-driven ocean, *J. Atmospheric Sci.* **20**, 594–606 (1963).
15. A. S. SARKISYAN, On the role of purely drift advection of density in the dynamics of wind-induced currents in a baroclinic ocean, *Bull. Acad. Sci. USSR, Geophys. Ser.* No. 9, 911–917 (1961).
16. Z. F. ZORIKOVA, On the calculation of currents in the surface layer in the northern sector of the Pacific, *Bull. Akad. Sci. USSR, Geophys. Ser.*, No. 9, 776–781 (1962).
17. Y. K. GORMATYUK AND A. S. SARKISYAN, Results of four-level model calculations of North Atlantic currents," *Akad. Sci. USSR Izvestiya Atmospheric Oceanic Phys.* **1**, 185–191 (1965).
18. W. GATES, A numerical study of transient rossby waves in a wind-driven homogenous ocean, *J. Atmospheric Sci.* **25**, 3–22 (1968).
19. G. VERONIS, Wind driven ocean circulation. II. Numerical solutions of the non-linear problem, *Deep Sea Res.* **13**, 31–56 (1966).
20. K. BRYAN AND M. COX, A numerical investigation of the oceanic general circulation, *Tellus* **19**, 54–80 (1967).
21. O. MAMAEV, A Simplified relationship between density, temperature and salinity of sea water, *Bull. Akad. Sci. Geophys. Ser., No.* 2, 180–181 (1964).
22. G. NEUMANN AND W. PIERSON, "Principles of Physical Oceanography," p. 42. Prentice Hall, Englewood Cliffs, New Jersey (1966).
23. A. PIVOVAROV, Effect of solar radiation penetrating into the sea in forming the water temperature, *Okeanologiya* **3**, 213–218 (1963).
24. L. LANDAU AND E. LIFSHITZ, "Fluid Mechanics." Addison Wesley, Reading, Massachusetts (1959).
25. O. MAMAYEV, The influence of stratification on vertical turbulent mixing in the sea, *Bull. Akad. Sci. USSR. Geophys. Ser., No.* 7, 494–497 (1958).
26. W. MUNK AND E. ANDERSON, Notes on a theory of the thermocline, *J. Marine Res.* **7**, 276–295 (1948).

27. O. M. PHILLIPS, "The Dynamics of the Upper Ocean." Cambridge University Press, (1966).
28. H. GRANT, R. STEWART, AND A. MOILLIET, Turbulence spectra from a tidal channel, *J. Fluid. Mech.* **12**, 241–268 (1961).
29. N. PINUS, E. REITER, G. SHUR, AND N. VINNICHENKO, Power spectra of turbulence in the free atmosphere, *Tellus* **19**, 206–213 (1967).
30. R. FJØRTOFT, On the changes in the spectral distribution of kinetic energy for two dimensional nondivergent flow, *Tellus* **5**, 225–230 (1953).
31. R. KRAICHNAN, Inertial ranges in two-dimensional turbulence, *Phys. Fluids* **10**, 1417–1423 (1967).
32. C. LEITH, Diffusion approximation for two-dimensional turbulence, *Phys. Fluids*, **11**, 671–672 (1968).
33. C. LEITH, Lawrence Radiation Laboratory, Livermore (private communication, 1967).
34. G. MARCHUK, Theoretical model for weather forecasting, *Dokl. Akad. SSSR* **155**, 1062–1065 (1964).
35. R. RICHTMYER, "Difference Methods for Initial Value Problems." Interscience Publishers, New York (1957).
36. P. LAX, Numerical solution of partial differential equations, *Am. Math. Monthly* **72**, 74–84 (1965).
37. W. CROWLEY, Numerical advection experiments, *Monthly Weather Rev.* **96**, 1–11 (1968).